First-Principles Calculations of the Adsorption of Nitromethane and 1,1-Diamino-2,2-dinitroethylene (FOX-7) Molecules on the α-Al_2O_3(0001) Surface

Dan C. Sorescu,[†] Jerry A. Boatz,[‡] and Donald L. Thompson*[,§]

U.S. Department of Energy, National Energy Technology Laboratory, P.O. Box 10940, Pittsburgh, Pennsylvania 15236, Air Force Research Laboratory, AFRL/PRSP, Edwards AFB, California 93524, and Department of Chemistry, University of Missouri, Columbia, Missouri 65211

Received: August 23, 2004; In Final Form: October 20, 2004

First-principles calculations based on density functional theory (DFT) and the generalized gradient approximation (GGA) have been used to study the adsorption of nitromethane (NM) and 1,1-diamino-2,2-dinitroethylene (FOX-7) molecules on the basal plane of an α-Al_2O_3 crystal. The calculations employ a (2 × 2) supercell slab model and 3D periodic boundary conditions. On the basis of these calculations, we have determined that both NM and FOX-7 molecules can adsorb nondissociatively on the surface with the most stable adsorption configurations parallel to the surface. The binding energies are in the range 25.3−26.0 kcal/mol for NM and 35.6−48.3 kcal/mol for FOX-7 depending on the relative molecular orientation and the surface sites. The minimum energy pathways for NM dissociation have been determined, and a low-energy pathway leading to H-atom elimination with formation of adsorbed CH_2NO_2 and hydroxyl species has been identified. Additional calculations have focused on adsorption properties of *aci*-nitromethane tautomers and on description of the energetic pathways connecting adsorbed nitromethane molecule with these tautomers.

I. Introduction

The interaction of powderized aluminum with energetic materials represents a topic of significant interest as such materials can be used as energetic ingredients in rocket propellant formulations.[1] Its primary roles in energetic materials formulations include increasing the combustion exothermicity and the regression rate of solid propellant grains and enhancing the blasting effect of explosives.[2] Moreover, aluminum particles have been found to have beneficial effects by reducing the combustion instabilities in rocket motors.[2,3] The efficiency of such processes depends on the size of the Al particles. For example, in the case of Al nanopowders, significant improvements in the performance of some energetic materials over the common micron-size Al powders have been reported.[4,5]

Besides energetic materials applications, the interaction of nitromethane with oxides has also attracted the interest of the catalysis community. Nitromethane has been considered as a prototypical compound whose study can help to elucidate the reaction mechanism of catalytic reduction of nitric oxides by hydrocarbons under oxygen-rich conditions.[6−8] Yamaguchi[6] has reported thermal decomposition studies of nitromethane (NM) adsorbed on γ-alumina, pretreated at 773 K, based on infrared spectroscopy, NMR spectroscopy, and temperature-programmed desorption (TPD) measurements. He found that at room temperature NM adsorbs both molecularly (undissociated) in a weakly physisorbed state as well as in a dissociated state as *aci*-anion nitromethane (*aa*-NM, $CH_2NO_2^-$). It was suggested[6] that *aa*-NM may be formed as a result of the interaction between NM and the oxide surface, with formation of a surface hydroxyl group via the reaction $CH_3NO_2 + O^{2-} \rightarrow CH_2NO_2^- + OH^-$. The *aa*-NM species was found to remain stable on the surface up to $T = 373$ K. Above this temperature, two intermediate species were formed by decomposition of the *aci*-anion. These were tentatively assigned to nitrosoaldehyde and a (C,N,O) adduct intermediate formed by deprotonation and polymerization of *aa*-NM:

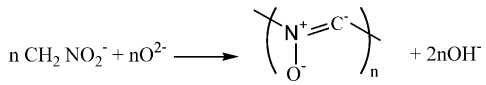

Above 373 K, these intermediate species may further decompose to form isocyanate.

Formation of *aci*-anion nitromethane upon adsorption of nitromethane on a variety of oxides with basic sites has been confirmed by Lima et al.[8] Using ^{13}C CP/MAS NMR, they have shown that in the cases of γ-Al_2O_3, MgO, and Mg(Al)O oxides, proton abstraction by basic sites leads to formation of *aa*-NM, which is stabilized by the conjugate Lewis acid site. Moreover, they identify a direct correlation between the chemical shift of the carbon atom of adsorbed nitromethane and the heat of adsorption of CO_2 on the same material. As this heat of adsorption is proportional to the basicity of the surface sites, Lima et al.[8] have shown that NM can be used as an accurate NMR probe for monitoring the basicity of oxide surfaces.

The results obtained by these groups[6,8] indicate that, upon adsorption on alumina, surface decomposition of NM can take place at relatively low temperatures, below 373 K. Moreover, specific processes such as the rearrangement reaction of NM with formation of *aci*-nitromethane (*a*-NM) or deprotonation reactions of *a*-NM can play important roles in the chemistry of NM on the aluminum oxide surface. However, the precise mechanism of these reactions and formation of *a*-NM and *aa*-NM compounds is not yet available. Despite the experimental interest in understanding the catalytic properties of nitro compounds on alumina, to the best of our knowledge, no

* Corresponding author.
[†] U.S. Department of Energy.
[‡] Air Force Research Laboratory.
[§] University of Missouri.

10.1021/jp046193k CCC: $30.25
Published on Web 01/07/2005

theoretical studies are available to date. We note, however, some related work by Allouche.[9] By using ab initio cluster calculations, he investigated the adsorption of nitromethane on MgO(100) and CaO(100) surfaces and determined the catalytic action of these basic oxides on deprotonation reactions.

To clarify some of the fundamental issues related to the interactions of energetic materials, particularly nitro compounds, with the Al_2O_3 surface, in the present work, we focus on atomic-level descriptions of the interactions between the energetic compounds NM and 1,1-diamino-2,2-dinitroethylene (FOX-7) with the α-alumina surface. This study represents an extension of our recent density functional theory (DFT) results of the adsorption and decomposition of the same molecular systems, NM and FOX-7, on the Al(111) surface.[10] In that case, we determined that oxidation of the aluminum surface readily occurs by partial or complete dissociation of the oxygen atoms from the NO_2 groups in NM and FOX-7. In the case of dissociative chemisorption, abstraction of one or both O-atoms of a nitro group by Al surface atoms was seen to be the dominant mechanism. The dissociated oxygen atoms form strong Al−O bonds with the neighboring Al sites around the dissociation sites. Additionally, the radical species obtained as a result of oxygen atom elimination remain bonded to the surface.

In the current study, we analyze similar issues related to the adsorption of NM and FOX-7 on the aluminum oxide surface. In addition, as suggested by experimental studies, particularly in strongly basic solutions, the tautomeric form of NM, *aci*-nitromethane (*a*-NM), can also be seen as an adsorbed species on the oxide surface.[7] Our current study does not try to emulate the conditions found in liquid solutions. Rather, they correspond to experiments performed under ultrahigh vacuum conditions. Nevertheless, we have considered in the present work not only an analysis of the chemisorption properties of NM and FOX-7 but also the adsorption and decomposition properties of *a*-NM.

This paper is organized as follows: in section II, we describe the computational methods used to perform the adsorption calculations. The results and corresponding discussions of the total energy calculations for adsorption and dissociation of NM and *aci*-NM tautomers are presented in section III. In the same section, we analyze the corresponding results for the FOX-7 molecule. We summarize the main conclusions in section IV.

II. Computational Methods

The calculations performed in this study were done using the Vienna ab initio simulation package (VASP).[11−13] This program evaluates the total energy of periodically repeating geometries based on DFT and the pseudopotential approximation. In this case, the electron−ion interaction is described by fully nonlocal optimized ultrasoft pseudopotentials similar to those introduced by Vanderbilt.[14,15] Periodic boundary conditions are used, with the one-electron pseudo-orbitals expanded over a plane-wave basis set. The expansion includes all plane waves with kinetic energy $\hbar^2k^2/2m < E_{cut}$, where k is the wave vector, m is the electronic mass, and E_{cut} is the cutoff energy. In this study, a cutoff energy of 495 eV is chosen that ensures convergence with respect to the basis set.

Calculations were performed using the generalized gradient approximation (GGA) DFT with the PW91 exchange-correlation functional.[16] The sampling of the Brillouin zone was performed using a Monkhorst−Pack scheme.[17] The minimization of the electronic free energy was performed using an efficient iterative matrix-diagonalization routine based on a sequential band-by-band residuum minimization method (RMM)[12,13] or alternatively based on preconditioned band-by-band conjugate-gradient (CG) minimization.[18] The optimization of different atomic configurations was performed by conjugate-gradient minimization of the total energy.

The minimum energy paths between distinct minima were evaluated by use of the nudged elastic band (NEB) method of Jónsson and co-workers.[19] In this approach, the reaction path is "discretized", with the discrete configurations, or images, between minima being connected by elastic springs to prevent the images from sliding to the minima in the optimization.

III. Results and Discussion

A. Test Calculations for Bulk α-Al_2O_3 and Al_2O_3(0001) Surface. A number of tests have been initially performed to verify the accuracy of the method when applied to bulk Al_2O_3, the bare alumina surface, and to the isolated NM and FOX-7 molecules, and to clarify different technical aspects such as the optimum cutoff energy for these calculations.

The 10-atom rhombohedral primitive cell of α-Al_2O_3 has been optimized using a cutoff energy of 495 eV. In these calculations, a Monkhorst−Pack grid of 3 × 3 × 3 has been used, leading to 14 irreducible k-points in the Brillouin zone. Based on a fit of the dependence of the unit cell energy on the corresponding cell volume with the Murnaghan equation of state,[20] an optimum volume of the unit cell of 86.6076 Å^3 has been determined. This value is 2.2% higher than the experimental values reported by Wyckoff ($V_{o,exp}$ = 84.7116 Å^3)[21] and 1.7% higher than that of d'Amour et al.[22] ($V_{0,exp}$ = 85.1087 Å^3). The corresponding rhombohedral unit parameters are a_{calc} = 5.162 Å and α_{calc} = 55.27°. These values are within 0.5% of the experimental values of a_{exp} = 5.136 Å and α_{exp} = 55.30°, measured by d'Amour et al.[22] The positions of the Al- and O-ions were calculated to be u(Al) = 0.352 and u(O) = 0.556, which are essentially identical to those obtained experimentally.[21] The bulk modulus at zero pressure and its pressure derivative obtained from a Murnaghan analysis were $B_{0,calc}$ = 2.31 Mbar and $B'_{0,calc}$ = 3.92. The corresponding values reported by d'Amour et al.[22] were $B_{0,exp}$ = 2.54 Mbar and $B'_{0,exp}$ = 4.27. Finally, the cohesive energy of the rhombohedral unit cell per Al_2O_3 unit was determined to be 31.52 eV, which is very close to the experimental value of 31.8 eV.[23] These results indicate that the present set of pseudopotentials is able to provide a very good representation of the structural and energetic properties of bulk Al_2O_3.

The surface model employed in this study corresponds to the (0001) basal plane of α-Al_2O_3. Using the optimized unit cell values, a supercell model was constructed containing 2 × 2 surface units with three layers of O atoms (36 ions) and six layers of Al atoms (24 ions). The surface slab is separated by a vacuum layer of 12 Å from the neighboring slabs in the direction perpendicular to the surface. It has been shown in previous studies that an Al-terminated Al_2O_3(0001) surface is energetically the most stable.[24,25] Consequently, we adopt the same surface termination in the present work. A 3 × 3 × 1 Monkhorst−Pack grid of k-points has been used in optimization calculations.

Initial surface optimizations have been performed by relaxing all ions in the systems. We have determined that the surface energy decreases from the 3.58 J/m^2 corresponding to the unrelaxed structure to 1.51 J/m^2 after relaxation. This significant reduction of surface energy by a factor well over 2 was also noted by Manassidis et al.[24] based on LDA calculations. Our surface energy is basically identical to that obtained by Jarvis et al.[25] of 1.5 J/m^2 using DFT-GGA calculations and only slightly larger than the value of 1.42 J/m^2 obtained on the basis of the same computational method by Alavi et al.[26] As a result of surface optimization, significant inward relaxations of about 0.8 Å take place for the surface Al atoms, which are positioned

TABLE 1: Comparison of the Calculated Geometric Parameters for Nitromethane and *aci*-Nitromethane to the Previously Reported Experimental[a] and Theoretical[b] Values

parameter[c]	NM staggered	NM eclipsed	NM exp.[a]	*aci*-NM *cis*	*aci*-NM *cis*, theor.[b]	*aci*-NM *trans*
r(C−N)	1.498	1.497	1.489	1.302	1.313	1.309
r(N−O_1)	1.241	1.240	1.224	1.448	1.425	1.467
r(N−O_2)	1.241	1.240	1.224	1.248	1.236	1.232
r(C−H_1)	1.094	1.089	1.088			
r(C−H_2)	1.090	1.093	1.088	1.080	1.077	1.081
r(C−H_3)	1.090	1.093	1.088	1.080	1.076	1.081
r(O−H_1)				0.983	0.981	0.981
Θ(O_1NO_2)	125.6	125.6	125.3	115.4	115.8	112.6
Θ(CNO_1)	117.2	117.8	117.3	113.6		117.1
Θ(CNO_2)	117.2	116.6	117.3	131.0	131.2	130.2
Θ(NCH_1)	106.6	108.7	107.5			
Θ(NCH_2)	108.3	107.1	107.5	118.3	116.3	120.2
Θ(NCH_3)	108.3	107.1	107.5	116.8	118.1	116.7
Θ(NOH_1)				99.7	99.5	105.7
ΔE	0.0	0.029		11.857		17.654

[a] Microwave experimental data from Jeffrey et al., ref 31. [b] MP2/6-311+G* results from Lammertsma and Prasad, ref 28. [c] Bond distances are given in angstroms, bond angles in degrees, and relative energies ΔE in kcal/mol.

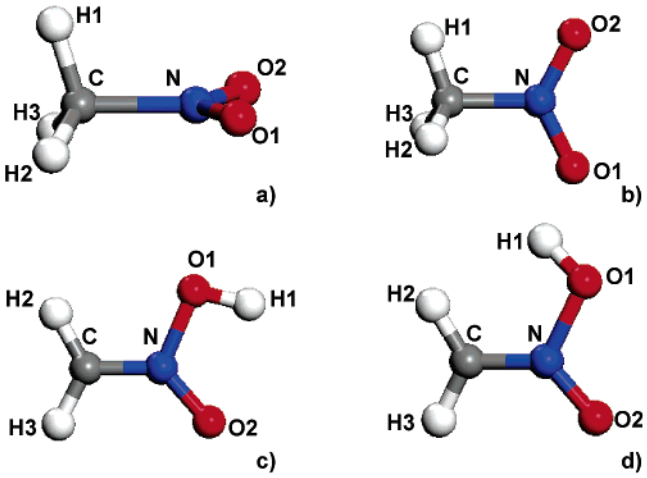

Figure 1. Structural configurations of staggered (a) and eclipsed (b) nitromethane and of the *cis* (c) and *trans* (d) *aci*-nitromethane molecules.

almost in the same plane with the O atoms. The vertical separation between the top plane of Al atoms and the immediate next plane of O atoms is only 0.04 Å. For the surface top layer, the Al−O bonds decrease from the bulk value of 1.87 to 1.69 Å. These values are close to those reported by Jarvis et al.[25] and Alavi et al.[26]

B. Test Calculations for Isolated NM and FOX-7 Molecules. In a previous study[27] dedicated to analysis of the structural and electronic properties of crystalline FOX-7, we have shown that plane-wave DFT calculations using the VASP code can be used to provide an accurate description of the structural properties of this molecule as well as of the corresponding crystal structure. The details of this analysis will not be repeated here. In this section, we will only focus upon results related to the gas-phase nitromethane tautomers, which can interact with the Al_2O_3 surface.

Isolated NM and *aci*-NM molecules have been optimized in a cubic box of 12 × 12 × 12 Å^3. For nitromethane, both the staggered and the eclipsed conformations (see Figure 1a and b) have been considered. Similarly, for the *aci* form of nitromethane, CH_2═NO_2H, we have analyzed both the *cis* and the *trans* configurations (see Figure 1c and d). The corresponding structural and energetic parameters are given in Table 1. From the analysis of the energetic data given in Table 1, it can be seen that the staggered and eclipsed conformations of NM have almost identical energies, with an extremely small difference of 0.029 kcal/mol. This result is similar to that by Lammertsma et al.[28] based on ab initio calculations at MP2/6-31G*, MP4/6-31G*, and MP4/6-311+G** levels. They computed the energetic difference between the eclipsed and staggered configurations of NM to be 0.025 kcal/mol at the MP4/6-311+G** level, which is practically identical to the present result. Similarly, the energy difference between the staggered configuration of nitromethane and the *cis* configuration of *a*-NM (see Figure 1c) was computed by Lammertsma and Prasad[28,29] to be 14.14 kcal/mol at G1 or G2[30] levels of theory. Our calculations predict a difference of 11.9 kcal/mol, in good agreement with the previous high level ab initio results. Moreover, we found that in the case of the *aci*-NM molecule, the *cis* isomer is more stable than the *trans* isomer by 5.7 kcal/mol. This difference agrees well with the Lammertsma and Prasad result[29] of 6.7 kcal/mol, determined at the G2 level of theory.

The differences in the geometrical parameters of the staggered and eclipsed conformations of the NM molecule, summarized in Table 1, are minimal. Additionally, there is a good agreement between the predicted and experimental values[31] for the majority of geometric parameters. The largest deviation is seen in the N−O bond lengths, for which the computed values are about 1.3% larger than experiment. This slight overestimation is found in other ab initio predictions as well. For example, Lammertsma and Prasad[28] have calculated N−O bond lengths, r(N−O) = 1.24 Å, at the MP2/6-31G* level that are practically identical to those computed in the present study.

Good agreement also has been found between our calculated geometric parameters of *cis aci*-NM and those reported by Lammertsma and Prasad.[28] A comparison of these two sets of values is provided in Table 1. The largest difference of 0.023 Å is seen for the case of N−O1 bond of *aci*-NM. In the case of *trans aci*-NM isomer, optimized under C_s symmetry at the MP2/6-31G* level, Lammertsma and Prasad[28] found that this corresponds to a transition state. We have optimized the *trans aci*-NM isomer without imposing the C_s symmetry constraint. We found a local minimum corresponding to a structure where the H1 atom of *aci*-NM is out of the molecular plane (see Figure 1d), with a torsion angle τ(C−N−O1−H1) = −19.1°.

The agreement between our results for NM, FOX-7, and *cis a*-NM systems and either experimental values or other high-level ab initio calculations indicates that the present theoretical

TABLE 2: Representative Bond Geometries and Adsorption Energies for Nitromethane (NM), *aci*-Nitromethane (*a*-NM), and Dissociated Species (RNM) Adsorbed on the Al_2O_3(0001) Surface

parameter[a]	NM(**I**)	NM(**II**)	NM(**III**)	NM(**IV**)	NM(**V**)	*a*-NM (**I**)-*cis*	*a*-NM (**II**)-tr	*a*-NM (**III**)-*cis*	*a*-NM (IV)-tr	RNM1	RNM2
r(C−N)	1.481	1.484	1.484	1.478	1.477	1.288	1.284	1.286	1.291	1.316	1.312
r(N−O_1)	1.277	1.274	1.278	1.284	1.280	1.628	1.728	1.391	1.403	1.401	1.421
r(N−O_2)	1.217	1.218	1.217	1.219	1.219	1.219	1.207	1.303	1.287	1.247	1.245
r(C−H_1)	1.097	1.095	1.095	1.088	1.089						
r(C−H_2)	1.089	1.089	1.089	1.104	1.098	1.090	1.085	1.098	1.101	1.081	1.083
r(C−H_3)	1.091	1.091	1.092	1.097	1.097	1.085	1.087	1.083	1.084	1.082	1.082
r(O_1−H_1)						0.980	0.980	0.985	0.981	0.977	0.984
r(Al_1−O_1)	1.938	1.938	1.942	1.906	1.915	1.884	1.875	1.866	1.866	1.749	1.744
E_{ads}(1)[b]	19.8	19.6	19.1	26.0	25.3	24.2	22.4	31.5	31.1		
E_{ads}(2)						12.3	10.5	19.6	13.7		

[a] Bond distances are given in angstroms and binding energies in kcal/mol. The indices **I**−**V** for nitromethane correspond to the following structures: (**I**) Figure 2, panel a2; (**II**) Figure 2, panel b2; (**III**) Figure 2, panel c2; (**IV**) Figure 3, panels b and c; (**V**) Figure 3, panel d. The indices **I**−**IV** for *aci*-nitromethane correspond to the structures a−d represented in Figure 6, respectively. RNM1 and RNM2 represent the species obtained by H dissociation directly from NM (see Figure 5a, image 8) or from *a*-NM(**I**) (see Figure 9, image 8). [b] E_{ads}(1) (E_{ads}(2)) represents the binding energy with respect to the isolated slab and the corresponding isolated molecule (the isolated nitromethane molecule).

description of individual molecules and their isomers is adequate. Additionally, we have seen that good descriptions of both structural and energetic data for both the bulk oxide system and the bare surface are obtained. The accuracy of these theoretical predictions lends confidence to the next step of our investigation, the interactions of NM and FOX-7 molecules with the Al_2O_3(0001) surface.

C. Nitromethane Adsorption on Al_2O_3(0001) Surface. C1. Geometries and Energies. The adsorption studies of NM on the α-Al_2O_3(0001) surface were done using the 2 × 2 supercell described above. Adsorptions at several surface sites and for distinct orientations of the NM molecule relative to the surface were first examined. The adsorption energies calculated throughout this work were obtained on the basis of the expression

$$E_{ads} = E_{molec} + E_{slab} - E_{(molec+slab)} \quad (1)$$

where E_{molec} is the energy of the isolated adsorbate molecule in its equilibrium position, E_{slab} is the total energy of the slab, and $E_{(molec+slab)}$ is the total energy of the adsorbate/slab system. A positive E_{ads} corresponds to a stable adsorbate/slab system. The energy of the isolated adsorbate molecule was determined from calculations performed on a single molecule in a cubic cell with sides of 12 Å. The same Brillouin-zone sampling has been used to calculate the energies of the bare slab and of the molecule-slab systems.

The first set of adsorption configurations we investigated corresponds to the case in which the NM molecule is adsorbed with the C−N bond perpendicular to the surface and the nitro group oriented toward the surface. Several initial positions of the molecule on the surface were considered, of which three representative configurations are depicted in Figure 2. Panels a1−c1 in Figure 2 show the initial starting configuration, while panels a2−c2 show the final, optimized configurations. For clarity and ease of notation, these final configurations will be denoted as NM(**I**), NM(**II**), and NM(**III**), respectively. In the optimization process, all of the atoms of the slab model and of the NM molecule were allowed to relax, with the exception of the bottom Al and O layers of the slab. In panels a1−c1 of Figure 2, we illustrate the cases in which the NM molecule was placed initially on top of O and Al atoms of the surface or above a fcc hollow site. As indicated in panels a2−c2 of Figure 2, independent of the initial configuration of the NM molecule, adsorption on the surface takes place by initial bonding of one of the oxygen atoms of the nitro group to an Al atom of the surface. The geometric parameters of the NM molecule adsorbed on the surface for each of the three optimized configurations

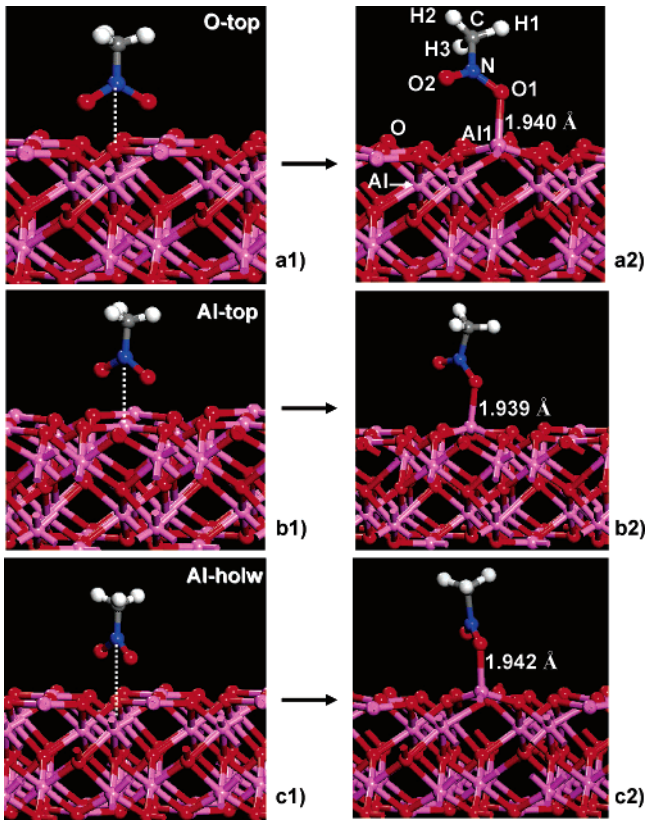

Figure 2. Adsorption configurations of NM on the Al_2O_3(0001) surface obtained from initial vertical configurations: (a) N above an O atom (NM(**I**)); (b) N above an Al atom (NM(**II**)); and (c) N above a hollow site (NM(**III**)). The initial configurations are depicted in panels a1−c1, while the corresponding optimized configurations are presented in panels a2−c2, respectively.

depicted in Figure 2 are given in Table 2, together with the corresponding calculated binding energies. For all of these vertical configurations, the binding energies have similar values in the range 19.1−19.8 kcal/mol. The lengths of the Al−O bonds formed upon adsorption range between 1.938 and 1.942 Å. Relative to the isolated molecule, the N−O1 bond involved in bonding to the surface is stretched by about 0.034−0.038 Å, while the other N−O2 bond is slightly compressed by 0.02 Å. The existence of a strong interaction between NM and the oxide surface is also reflected by an upward shift of 0.63−0.71 Å of the surface A11 atom involved in bonding relative to the initial relaxed surface structure.

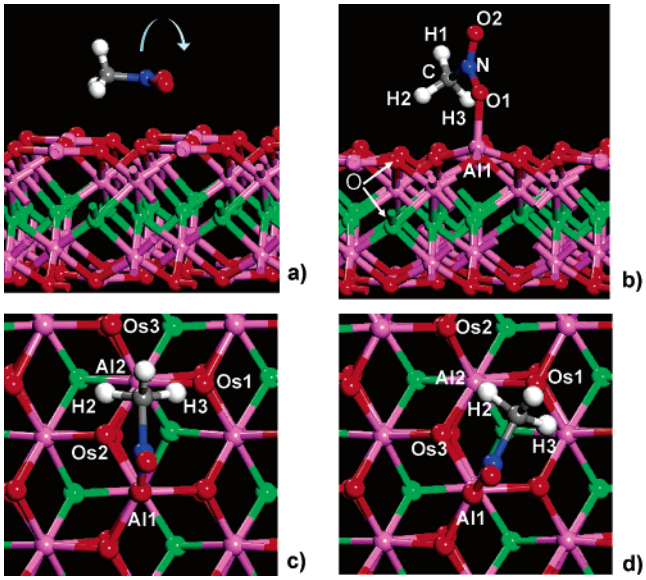

Figure 3. (a−c) Adsorption configuration of NM on the $Al_2O_3(0001)$ surface obtained from an initial parallel configuration with the NO_2 group taken parallel to the surface. The initial configuration is depicted in panel a, while the corresponding final configuration is presented in panels b (lateral view) and c (top view). The direction of the C−N bond is parallel to the Al1···Al2 direction. Panel d depicts another possible adsorption configuration of NM, where the C−N bond is parallel to the Al1···Os1 direction. In all of these figures, the O and Al atoms are colored in red and pink, respectively. For clarity, the O atoms in the second layer are shown in green.

We have also investigated the case where the NM molecule was initially oriented perpendicular to the surface but with the methyl group directed toward the surface (not shown). We have analyzed two cases: one in which the C−N bond was positioned above an Al atom and the other one above an O atom from the top layer. For both of these two configurations, we have determined only very weak adsorption minima with binding energies between 0.97 and 1.13 kcal/mol. Consequently, NM adsorption with the methyl group directed toward the surface is not favorable and has not been pursued further in this study.

Another set of optimizations has been done in which the initial configuration of the NM molecule has both the C−N bond and the NO_2 group parallel to the surface. Several cases were tested in which the initial position of the N atom was placed either above an Al or O atom of the surface or above the hollow sites. The final results are similar, and we present a representative case, denoted hereafter as NM(**IV**), in Figure 3. As indicated in this figure, during the optimization process, the nitro group, initially parallel to the surface (see Figure 3a), rotates to minimize the repulsive interactions with O atoms of the surface. In the final configuration (see Figure 3b and c), the nitro group is practically perpendicular to the surface plane, leading to an eclipsed conformation of the NM molecule. In this configuration, the major binding of the molecule to the surface takes place through the Al1−O1 bond. Additionally, as illustrated in Figure 3c where a top view of the adsorption configuration of NM(**IV**) structure is shown, two of the H atoms of the methyl group are directly pointing to the surface O atoms (see, for example, the atoms H3 and surface Os1 atom in Figure 3c), indicating a weak attractive interaction. Using notation from Figure 3c, the corresponding H...O distances are: r(H3−Os1) = 2.126 Å, r(H2−Os2) = 2.399 Å, and r(H2−Os3) = 2.752 Å. In this parallel adsorption configuration, the binding energy of the NM molecule increases to 26 kcal/mol. This value is about 7 kcal/mol higher than the one determined for the vertical adsorption configuration, indicating a more stable adsorption configuration. This energetic increase is also reflected in the modifications of the molecular geometric parameters given in Table 2. Relative to the vertical configurations, the most significant change in the parallel configuration is in the Al1−O1 bond, which decreases from about 1.94 Å in NM(**I**,**II**,**III**) to 1.906 Å in NM(**IV**). The corresponding N−O1 bond is stretched to 1.284 Å, and slight elongations of C−H bonds to 1.097−1.104 Å are present due to the attractive interactions of the H atoms with the surface oxygen atoms.

As illustrated in Figure 3c, the C−N bond of the NM(**IV**) structure is essentially oriented along the Al1···Al2 direction. We have tested also the case where the C−N bond is aligned along the Al1···Os1 direction as presented in Figure 3d. In this case, for the final optimized structure, NM(**V**), none of the H atoms of the methyl group are pointing directly toward O atoms of the surface. The closest H...O distances are r(H3−Os1) = 2.487 Å and r(H2−Os1) = 2.566 Å. The binding energy of this structure, 25.3 kcal/mol, is slightly smaller than that for NM(**IV**).

C2. Electrostatic Charges. A common tool for obtaining a semiquantitative measure of charge transfer is the Mulliken population analysis[32] in which the electronic charge is partitioned among the individual atoms. This partitioning has been done in the present study using the periodic boundary condition version of the DFT program DMOL^3 developed by Delley.[33,34] DMOL^3 uses a basis set of numeric atomic functions that are exact solutions to the Kohn−Sham equations for the atoms. Calculations have been done using a double numeric polarized (DNP) basis set and the nonlocal Perdew−Wang (PW91) functional within generalized-gradient approximation.[35] The geometrical structures obtained in VASP calculations were transferred without modifications to perform DMOL^3 calculations. The Mulliken charges for the isolated NM molecule in both the staggered and the eclipsed configurations and for the vertical (NM(**II**)) and parallel (NM(**IV**)) adsorption configurations are summarized in Table 3. As expected, the largest changes in atomic charges are found for the O atoms of the nitro group. The charge of the O atom involved in Al−O bonding decreases from −0.31e for the isolated NM molecule to −0.39e for NM(**II**) and −0.40e for NM(**IV**), respectively. The charge of the other O atom of the nitro group has a reverse variation. Specifically, its charge becomes less negative, ranging from −0.31e in the gas phase to −0.19e for NM(**II**) and −0.2e for NM(**IV**). Concomitantly, the positive charge of the Al atom involved in bonding increases slightly from 1.11e for the isolated slab to 1.28e for NM(**II**) and 1.30e for NM(**IV**). The interaction of NM with the surface also leads to a net increase of the positive charge of H atoms. Specifically, from values around 0.12e corresponding to the isolated molecule, the H-atom charge increases to 0.16−0.17e in the vertical upward configuration and to about 0.2 e for the H atoms closest to the surface for the parallel adsorption configuration. These changes reflect the fact that the major interaction with the surface takes place through one of the O atoms of the nitro group, with a small contribution due to polarization of the H atoms of the methyl group.

The above changes can be put into better perspective if we compare them to those observed in the interactions of NM with the Al(111) surface.[10] In that study, it was shown that even in the case of nondissociative adsorption, there is a significant increase in the negative charge of the O atoms in NM of about −0.3e relative to the gas phase. A similar decrease of about 0.4e was found to take place in the positive charge of the N

TABLE 3: Variation of Mulliken Charges for Nitromethane and *aci*-Nitromethane Species in the Gas Phase and Adsorbed on the Al_2O_3(0001) Surface[a]

system	C	N	O1	O2	H1	H2	H3	Al	Os1	Os2	Os3
NM(gas,stag.)	−0.083	0.329	−0.306	−0.306	0.125	0.120	0.120				
NM(gas,eclips)	−0.082	0.329	−0.308	−0.304	0.118	0.124	0.124				
a-NM(gas,*cis*)	−0.087	0.324	−0.389	−0.350	0.284	0.109	0.109				
a-NM(gas,*trans*)	−0.120	0.325	−0.333	−0.341	0.268	0.111	0.090				
aa-NM(gas)	−0.203	0.355	−0.569	−0.569		−0.007	−0.007				
slab								1.109	−0.894	−0.894	−0.895
NM(**II**)	−0.151	0.362	−0.390	−0.190	0.171	0.162	0.170	1.280	−0.929	−0.929	−0.926
NM(**IV**)	−0.246	0.338	−0.403	−0.197	0.169	0.208	0.204	1.297	−0.948	−0.924	−0.934
RNM1	−0.232	0.361	−0.572	−0.372	0.327	0.140	0.107	1.357	−0.983	−1.000	−0.916
a-NM(**I**)	−0.122	0.287	−0.503	−0.253	0.327	0.221	0.155	1.311	−0.926	−0.933	−0.937
a-NM(**II**)	−0.109	0.249	−0.525	−0.184	0.320	0.224	0.155	1.319	−0.955	−0.926	−0.933
a-NM(**III**)	−0.105	0.356	−0.512	−0.286	0.318	0.238	0.153	1.286	−0.936	−0.926	−0.940
a-NM(**IV**)	−0.136	0.347	−0.453	−0.262	0.292	0.243	0.135	1.278	−0.938	−0.926	−0.942
RNM2	−0.228	0.344	−0.578	−0.355	0.361	0.153	0.123	1.317	−0.829	−0.946	−0.948

[a] Atomic labels for isolated and chemisorbed molecules are those indicated in Figues 1, 2, 3, 6 and 9. In case of NM adsorbed species, H2, H3, and O1 atoms are pointing to the surface. In the case of *aci*-NM species, H1 denotes the hydrogen atom bonded to O atom of nitro group and H2 and O1 atoms are pointing to the surface. The labels Os1, Os2, and Os3 denote the three surface oxygen atoms bonded to the Al1 surface atom where molecular bonding takes place.

atom. Naturally, with this transfer of electrons to the NM molecule, there is a corresponding increase in the positive charge of the Al atoms bonded to the NM molecule, with values in the range 0.38−0.51e. It can be concluded that, in the case of the oxide surface, the transfer of charge is smaller than in the case of the metallic surface. This observation is also consistent with the lack of dissociative chemisorption of the NM molecule adsorbed on the oxide surface, in contradistinction to the case of metallic Al surface.

C3. Minimum Energy Potential Path for Adsorbate Interconversion. As described in the previous section, adsorption of nitromethane can take place through two main configurations: (a) a vertical orientation in which bonding takes place between the O atom of the nitro group and an Al atom of the surface, and (b) a parallel configuration where contributions to surface bonding are provided by both the O atom of the nitro group and some of the H atoms of the methyl group. In this section, computations of the reaction pathway and energy necessary for interconversion between these two adsorbate configurations are described. Such calculations have been done using the NEB method where the initial and final states correspond to the vertical and parallel adsorption configurations, respectively. The results of these calculations are depicted in Figure 4. As seen in this figure, the potential energy surface in the region of upright configuration is very shallow. The activation energy is only about 1.8 kcal/mol for the interconversion from the upright to the parallel configuration. These results indicate that the upright configuration is only a metastable minimum on the potential energy surface. Upon initial bonding of the nitromethane to one of the Al surface atoms, rotation around the corresponding N−O bond (for the O atom involved in direct bonding to Al) can easily take place, leading to the more stable parallel configuration.

C4. Minimum Energy Path for NM Dissociation. Starting from the parallel adsorption configuration of NM on Al_2O_3(0001) surface (NM(**IV**)), we have analyzed two minimum energy pathways for molecular dissociation. The first corresponds to CH bond scission with formation of a surface OH bond. The second pathway corresponds to the C−N bond dissociation with formation of adsorbed CH_3 and NO_2 species. In both cases, the calculations of the minimum energy pathways were done using the NEB method for seven images distributed along the reaction pathway. The results are presented in Figure 5a and b. The initial and final adsorption configurations are depicted below the individual potential curves in Figure 5. The geometric parameters of the CH_2NO_2 species obtained by H elimination, denoted henceforth as RNM1, are provided in Table 2. In this case, nitromethyl species adsorbs through an Al−O bond with a length of 1.755 Å, while the newly formed hydroxyl group has a bond of 0.977 Å. The separation H1···C between the H atom of the newly formed hydroxyl group and the C atom from where dissociation took place is quite large, with a value of 3.237 Å. The total charge of the RNM1 species evaluated using the Mulliken charges given in Table 3 is −0.57e.

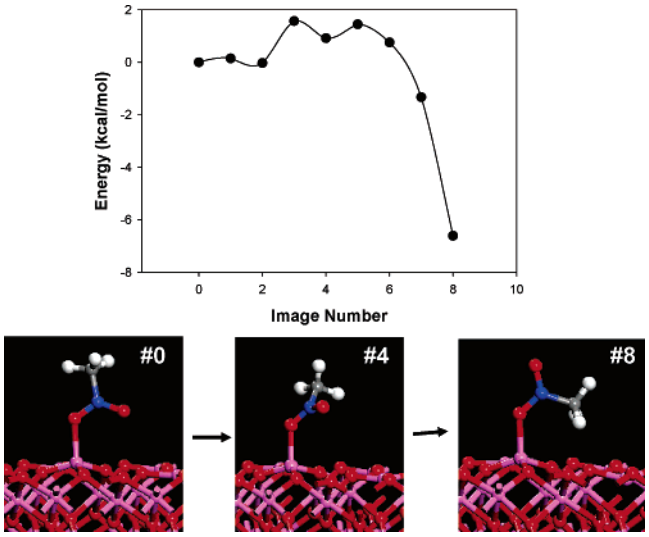

Figure 4. Minimum energy path for interconversion of the vertical NM(**III**) configuration to the parallel NM(**IV**) adsorption configuration. The indicated images correspond to the initial, intermediate local minimum, and final product configurations.

As can be seen from the plot 5a, the activation energy for the CH bond rupture reaction is about 13.8 kcal/mol. The other process, corresponding to C−N bond breaking, has a higher activation energy of about 37 kcal/mol. The activation energies of both reactions are significantly smaller than the corresponding energies for these reactions in the gas phase. For example, the C−H bond dissociation energy of gas-phase nitromethane was estimated to be 88.1 kcal/mol,[36] while for the C−N bond strength a value of 58.5 kcal/mol has been reported.[37] By comparing these values with our calculated NEB barriers, it follows that the Al_2O_3 surface significantly decreases the CH and CN bond dissociation energies in NM. The values of the activation energies presented above can be influenced by the

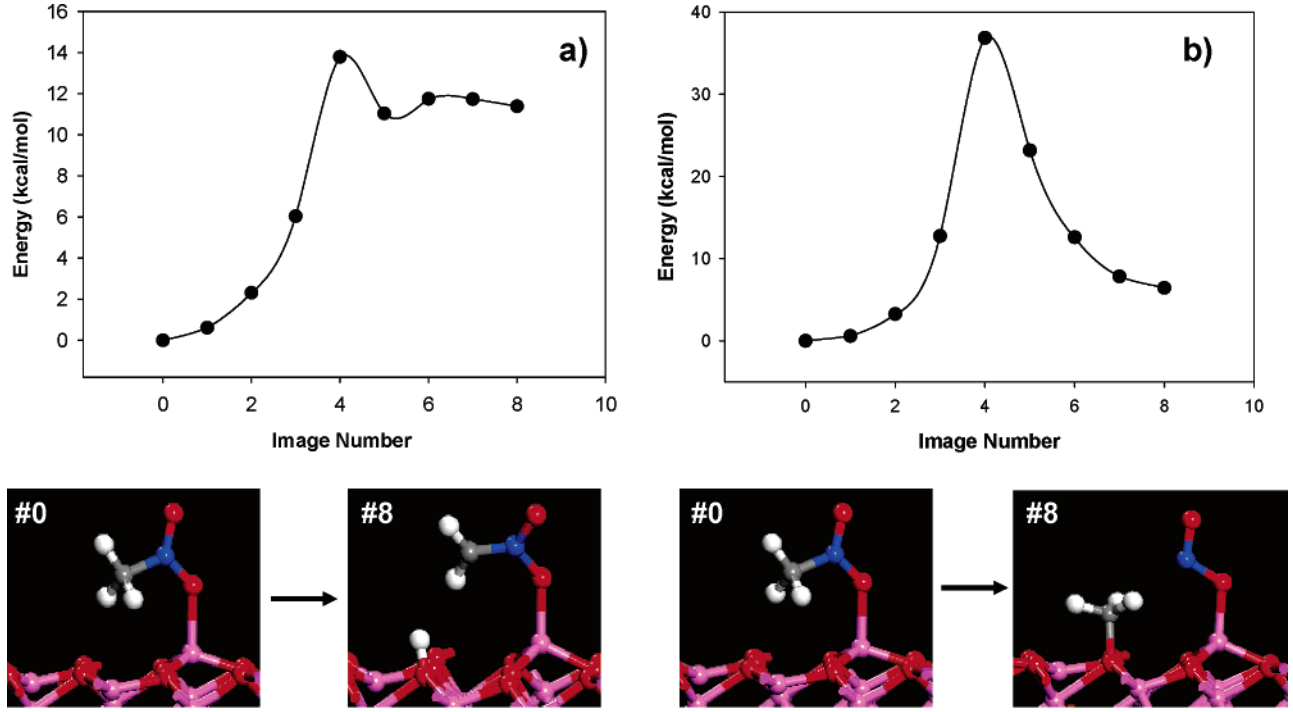

Figure 5. Minimum energy pathways for dissociation of the NM molecule starting from a parallel adsorbed configuration. Panel a corresponds to H scission from the methyl group with formation of adsorbed CH_2NO_2 and OH species. Panel b corresponds to C−N bond dissociation with formation of adsorbed CH_3 and NO_2 systems. The depicted atomic configurations correspond to the initial and final configurations of each reaction path.

presence of other coadsorbed species such as OH species. When OH groups are present on the surface, they will reduce the basicity of the surface, and as a result the activation energy for proton abstraction is expected to increase.

D. *aci*-Nitromethane Adsorption on Al_2O_3(0001) Surface. D1. Geometries and Energies. As was indicated in the Introduction, the formation of *aci*-nitromethane (*a*-NM) species on aluminum oxide surfaces has been inferred in several previous experimental studies, particularly on γ-alumina.[6,8] In this study, we have investigated the adsorption properties of both the *cis* and the *trans a*-NM species on α-Al_2O_3(0001). Here, the *cis* and *trans* forms differ in the orientation of the OH group relative to the NO bonds. For the adsorbed *a*-NM molecule, either the O atom that is bonded to the Al surface atom or the O atom pointing away from the surface can carry the hydroxyl group. Furthermore, each of these two isomers can exist in *cis* and *trans* forms, for a total of four possible configurations. Pictorial views of these configurations are given in Figure 6, while selected geometric parameters together with the corresponding binding energies are given in Table 2.

When the OH group is on the side of the *a*-NM molecule toward the surface (configuration *a*-NM(**I**) in Figure 6a), the binding energy of 24.2 kcal/mol is slightly smaller than that for NM(**IV**) (26.0 kcal/mol). This energy is evaluated with respect to the energies of the isolated slab and the isolated *cis* isomer of *a*-NM. However, when the binding energy is calculated with respect to the total energy of the isolated slab and of the isolated gas phase NM molecule, the corresponding value is only 12.3 kcal/mol. For the adsorbed *a*-NM, the molecular plane is perpendicular to the surface and contains the Al1−Os1 surface atoms. Such a configuration maximizes the attractive interactions between the O1···Al1, O1H1···Os1, and C−H2···Os2 pairs of atoms. At equilibrium, the O1−Al1 bond length is about 1.884 Å, while the distances from the H1 and H2 atoms to the closest O atoms of the surface are 2.822 and 2.209 Å, respectively. As in the case of parallel NM

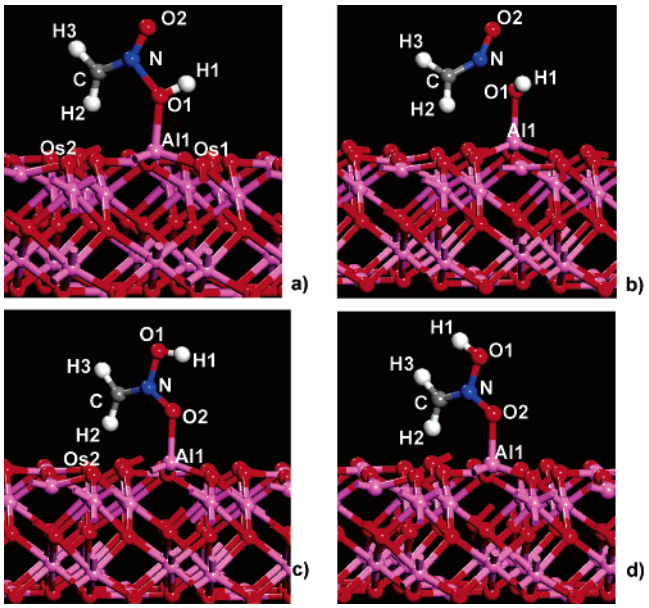

Figure 6. Adsorption configurations of *cis* and *trans aci*-nitromethane on the Al_2O_3(0001) surface. The panels a−d correspond to structures *a*-NM(**I**) to *a*-NM(**IV**) (see text), respectively.

adsorption, the Al atom bonded to *a*-NM is displaced above the surface by about 0.54 Å.

In addition to the *cis a*-NM(**I**) configuration, we have also obtained the optimized *trans a*-NM configuration, in which the OH group is on the side of the molecule facing the surface. The final configuration *a*-NM(**II**) is represented in Figure 6b. In this case, the O1H1 bond is rotated outward relative to the C−N−O1 plane with a torsional angle τ(C−N−O1−H1) = −100.04°. The total binding energy of this configuration is 1.8 kcal/mol smaller than that for the *a*-NM(**I**) structure. The most significant structural changes for the *cis a*-NM(**I**) and *trans a*-NM(**II**) configurations, relative to the corresponding geom-

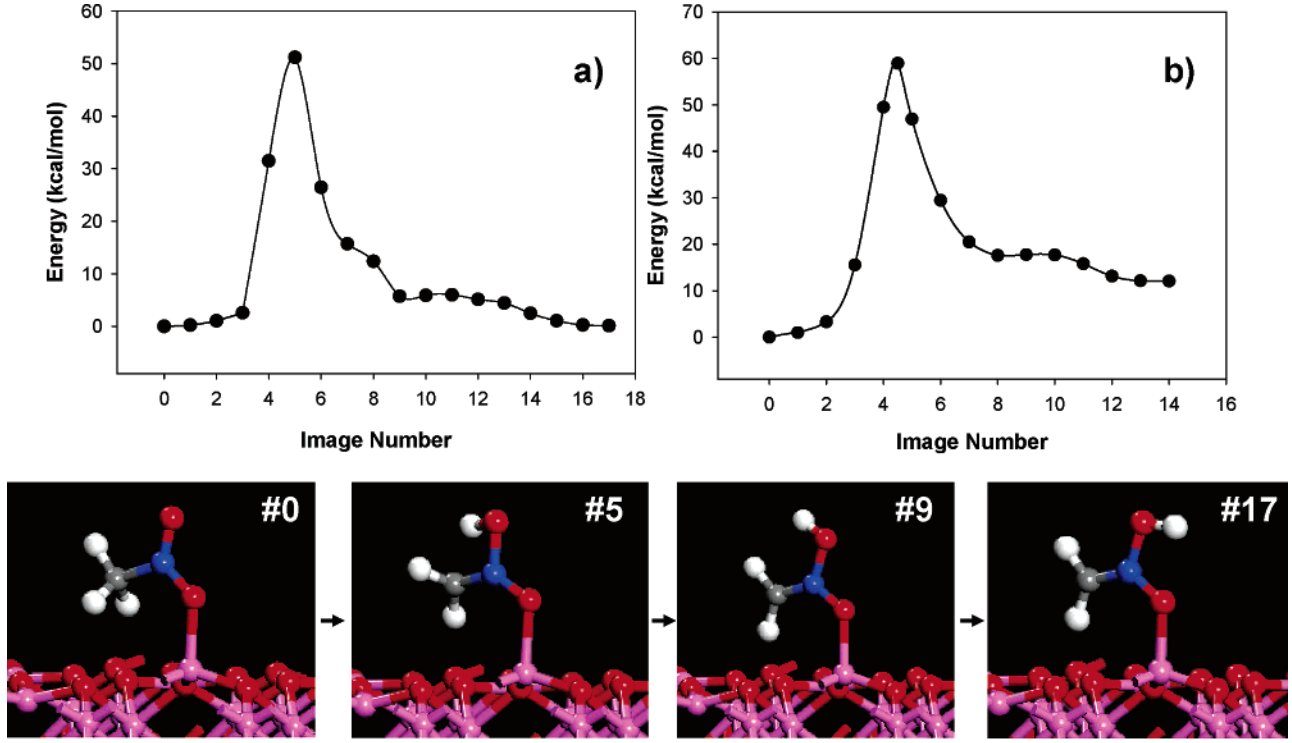

Figure 7. (a) Minimum energy reaction pathway for the tautomerization reaction NM(**IV**) → *a*-NM(**III**) on the Al_2O_3(0001) surface. The atomic configurations indicated at the bottom of the figure correspond to *a*-NM(**III**) (image 0), first transition state (image 5), *a*-NM(**IV**) (image 9), and *a*-NM(**III**) (image 17). Part b represents the minimum reaction pathway for NM → *trans a*-NM → *cis a*-NM reactions in the gas phase.

etries of the isolated *cis* and *trans a*-NM species, are the lengthening of the N−OH bonds, which reach values of 1.63 and 1.73 Å, respectively, indicating a significant weakening of this bond upon absorption on the surface. Note that subsequent analysis of the potential energy surface (presented in section D3) has indicated that this configuration is not a local minimum but rather a transition state.

Finally, the other two configurations we have analyzed correspond to *cis* and *trans* forms for the case when the OH bond is on the side of the nitro group pointing away from the surface. These configurations, denoted as *a*-NM(**III**) and *a*-NM(**IV**), are illustrated in Figure 6c and d. In these cases, the binding energies relative to the isolated NM molecule and the isolated surface are 19.6 and 13.7 kcal/mol for *cis* and *trans*, respectively. Therefore, among the four *a*-NM configurations, the *a*-NM(**III**) state corresponding to a *cis* tautomer with the OH group away from the surface is the most stable, followed by the *trans a*-NM(**IV**) tautomer. The increase in the binding energies of *a*-NM(**III**) and *a*-NM(**IV**) species is reflected also by a corresponding decrease of the Al1−O2 bond lengths to about 1.866 Å for both *cis* and *trans* tautomers. Similarly, the close contacts H2···Os2 decrease to 1.987 Å for *a*-NM(**III**) and 1.933 Å for *a*-NM(**IV**), respectively, while the lengths of the C−H bonds pointing toward the surface increase to 1.098 and 1.101 Å, respectively. Referring now to the intramolecular geometric parameters, the differences in the *cis a*-NM(**III**) and *trans a*-NM(**IV**) configurations include a lengthening of the N−OH bond from 1.391 Å in the former to 1.403 Å in the latter. Likewise, the length of the C−N bond increases from 1.286 to 1.291 Å. Such geometric variations have also been noted for the isolated gas-phase systems and have been associated with a repulsive electrostatic interaction between the *aci*-nitro hydrogen and the methylene group existent in the *trans* state.[28]

D2. Electrostatic Charges. On the basis of DMOL[3] calculations as described in section C2, we have calculated the Mulliken charges for the four *a*-NM tautomeric species. The results are listed in Table 3, including those obtained for the isolated molecules. By comparing the two sets of values, we notice that, as in the case of the NM molecule, the largest charge variations occur on the O− and H− atoms in the hydroxyl group. For the isolated *cis* and *trans* systems, the net charges on the hydroxyl group O- and H-atoms (O1 + H1 atoms in Table 3) are −0.105e and −0.065e, respectively. The corresponding values for adsorbed *cis* species are −0.176e for *a*-NM(**I**) and −0.194 for *a*-NM(**III**), while for the *trans* species they are −0.205e for *a*-NM(**II**) and −0.162e for *a*-NM(**IV**), respectively. More pronounced charge variations are seen for the H atom of the CH_2 group pointing to the surface (H2 atoms in Table 3) and for the Al atom involved in bonding to the molecule. The positive charge on the H atom increases by about 0.11e, while for the Al atom the increase is in the range 0.169−0.202e. Overall, the total charge transferred from *a*-NM(**III**) (0.162e) and *a*-NM(**IV**) (0.166e) to the surface is slightly larger than the charge transfer observed for *a*-NM(**I**) (0.112e) and *a*-NM(**II**) (0.13e), which is consistent with the larger binding energies for the two former tautomer configurations.

D3. Minimum Energy Potential Path for NM ↔ *aci*-NM Tautomerism and Dissociation of *a*-NM(I). In this section, we investigate the energetic requirements for the tautomeric reaction NM ↔ *aci*-NM taking place on the Al_2O_3(0001) surface. As previously discussed, several distinct adsorption configurations of *aci*-NM are found in which the OH group can be located on the side of *a*-NM either toward the surface or toward the vacuum side. In particular, we have considered two reaction pathways. The first one corresponds to the rearrangement reaction NM(**IV**) → *a*-NM(**III**) → *a*-NM(**IV**), while the second reaction corresponds to NM(**IV**) → *a*-NM(**II**) → *a*-NM(**I**).

The results of NEB calculations for the process NM(**IV**) → *a*-NM(**III**) → *a*-NM(**IV**) are illustrated in Figure 7a. Molecular structures corresponding to selected points along the reaction

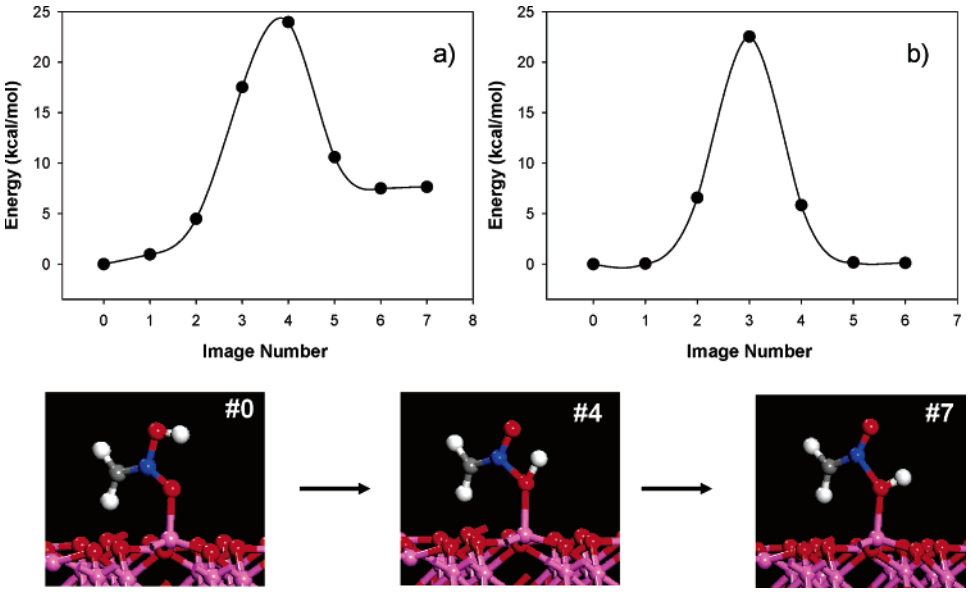

Figure 8. (a) Minimum energy reaction pathway for migration reaction of H between the *a*-NM(**III**) and *a*-NM(**I**) structures. The geometries of the initial configuration, the transition state, and the final configuration are depicted at the bottom of the figure. Panel b shows the energy profile for the same reaction in the gas phase.

pathway in Figure 7a are also represented at the bottom of this figure. Figure 7b shows the corresponding energy profile for the reaction in the gas phase. From Figure 7b, it is seen that the gas-phase tautomerization reaction NM → *trans a*-NM has an energy barrier of about 59 kcal/mol. From the *trans a*-NM configuration corresponding to image 8 in Figure 7b (not shown), the OH bond can further rotate to reach the *cis a*-NM (image 14 in Figure 7b) configuration with a very small activation energy of less than 0.2 kcal/mol. When the tautomerization reaction NM(**IV**) → *a*-NM(**III**) takes place on the Al_2O_3 (0001) surface, the results of our NEB calculations shown in Figure 7a indicate a decrease of the activation energy by about 8 kcal/mol to about 51 kcal/mol. As illustrated in Figure 7a, once the system reaches the *trans a*-NM(**IV**) state (image 9 in Figure 7a), the corresponding barrier to form *cis a*-NM(**III**) (image 17 in Figure 7a) is extremely small with a value of about 0.1 kcal/mol. From these calculations, it follows that if energy in excess of 51 kcal/mol is available, formation of *cis a*-NM(**III**) tautomer is possible.

We have also analyzed the potential energy surface for the tautomerization reaction NM(**IV**) → *a*-NM(**II**) → *a*-NM(**I**). On the basis of this analysis (not shown), we have found an activation energy of 56 kcal/mol, slightly larger than the one determined for NM(**IV**) → *a*-NM(**IV**) → *a*-NM(**III**). Additionally, the analysis of the potential surface around the NM(**II**) configuration indicates that this corresponds to a transition state rather than a local minimum.

Figure 8 shows the minimum energy pathways for the H-atom transfer reactions between the O atoms of the *cis a*-NM tautomers. As in the previous case, Figure 8a illustrates the case in which the reaction takes place on the surface (*a*-NM(**III**) → *a*-NM(**I**)), while Figure 8b corresponds to the case when reaction occurs in the gas phase. The atomic configurations depicted at the bottom of the figure correspond to the image numbers given in Figure 8a. As expected, the gas-phase reaction profile in Figure 8b is symmetric and the calculated activation energy is about 23 kcal/mol for H-atom migration between the O atoms of the nitro group. For the corresponding reaction on the surface (Figure 8a), the activation energy in the forward direction, *a*-NM(**III**) → *a*-NM(**I**), is not changed significantly ($E_b \approx 23.9$ kcal/mol.) However, the reverse process has a smaller activation energy of only 15.2 kcal/mol.

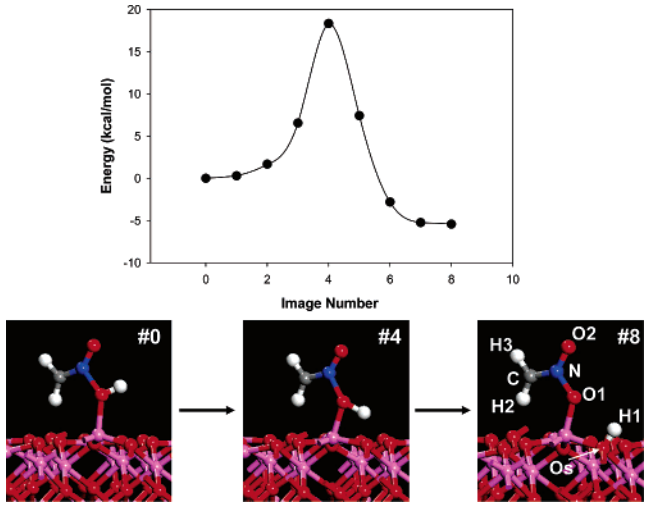

Figure 9. Minimum energy reaction pathway for dissociation reaction of *a*-NM(**I**) leading to adsorbed OH and CH_2NO_2(RNM2) species. The geometries corresponding to the initial, transition states, and final states are represented at the bottom of the figure.

Beside tautomerization reactions of NM, we have also analyzed an H-atom dissociation reaction of *a*-NM(**I**), for which the potential energy pathway is shown in Figure 9. In this process, the H1 atom of *a*-NM(**I**) migrates from the molecule to the surface, thereby breaking the O1−H1 bond and forming a new OH bond on the surface (denoted as Os−H1.) The resulting CH_2NO_2 species also remains adsorbed on the surface. The geometric parameters of this species, denoted henceforth as RNM2, are given in Table 2. The newly formed hydroxyl group has a bond length r(Os−H1) = 0.984 Å, while the separation between H1 and the oxygen O1 of the CH_2NO_2 species is r(O1···H1) = 2.544 Å. The RNM2 species adsorbs with an Al1−O1 bond of 1.744 Å, slightly smaller than the one for the RNM1 species obtained as a result of H dissociation from the NM molecule. Also, the total Mulliken charge of the RNM2 species (see Table 3) is −0.54e, similar to the one obtained for RNM1 species.

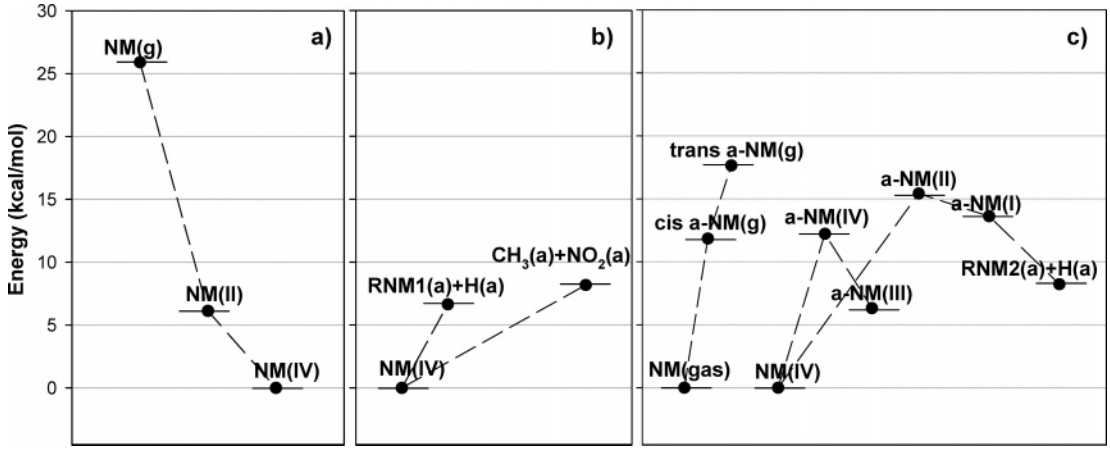

Figure 10. Relative energies for various configurations of adsorbed NM, *aci*-NM, and RNM species on $Al_2O_3(0001)$ surface. Panel a refers to NM adsorption. Panel b corresponds to the states obtained by direct dissociation of NM. Panel c presents two sets of data. The first corresponds to the relative energies of *cis* and *trans aci*-nitromethane in the gas phase with respect to gas-phase nitromethane. The second set indicates the relative energies of *cis* and *trans aci*-NM species adsorbed on the surface together with the energy of RNM2 species obtained by H dissociation from *a*-NM(**I**).

A summary of the calculated results for the adsorption, decomposition, and tautomerization reactions of NM on the $Al_2O_3(0001)$ surface is given in Figure 10. Panel a shows the relative energies of the gas phase and adsorbed configurations of NM. The adsorption process takes place via initial formation of the vertical configuration NM(**II**) followed by molecular reorientation leading to the parallel adsorption configuration, NM(**IV**). Panel b shows the relative energies of the configurations obtained by H-atom elimination, with subsequent formation of an adsorbed RNM1 species and a surface hydroxyl group, or by C−N bond dissociation with formation of adsorbed CH_3 and NO_2, from the adsorbed NM(**IV**) species. The total energy of the RNM1(a) + H(a) configuration, as well as the activation energy necessary to reach this state (evaluated in section C4) starting from adsorbed nitromethane, are smaller than those for the C−N dissociation pathway, indicating that the former process is both kinetically and thermodynamically more favorable than the latter. Finally, in panel c we present two sets of results. The first is a comparison of the relative energies of the *cis* and *trans aci*-NM species with respect to gas-phase NM (in staggered configuration). In the gas phase, *cis a*-NM(g) and *trans a*-NM(g) are less stable than NM(g) by 11.8 and 17.6 kcal/mol, respectively. For the adsorbed tautomeric *a*-NM species, two sets of results are obtained. When the OH group of *aci*-NM is far from the surface, that is, the *a*-NM(**III**) and *a*-NM(**IV**) configurations, the relative energies of these two species with respect to adsorbed nitromethane (NM(**IV**)) decrease to 6.3 and 12.2 kcal/mol. Therefore, the surface provides an additional stabilization of about 5.4−5.5 kcal/mol of the two tautomeric forms. However, when the OH group is close to the surface as in the case of the *cis a*-NM(**I**) configuration, the relative energy with respect to that of adsorbed NM increases to 13.6 kcal/mol. This corresponds to an increase in tautomerization energy relative to the gas phase. Finally, the energy RNM2(a) + H(a) of the species obtained from *aci*-NM(**I**) dissociation and of the adsorbed hydroxyl group is about 8.2 kcal/mol above the reference energy of adsorbed NM. This is slightly higher than the energy of the RNM1 + H(a) system of 6.6 kcal/mol.

E. FOX-7 Adsorption on the $Al_2O_3(0001)$ Surface. We have shown in previous sections that interactions of NM with the Al_2O_3 surface take place primarily through the nitro group, with formation of an Al−O bond. It is expected that similar mechanisms will also be found for other molecules containing the nitro chemical group. We have tested this in the present study for the case of the 1,1-diamino-2,2-dinitroethylene (FOX-7) molecule. The main interest for this compound is due to its applications as a high energy density material with superior shock-sensitivity properties.[38] In our previous study[10] of the interactions of nitro-containing molecules with an Al surface, we found very similar behavior for the NM and FOX-7 molecules. Particularly, we have found a common propensity for oxidation of the aluminum surface by these molecules through dissociation of the nitro groups and formation of strong Al−O bonds. Moreover, for NM and FOX-7, we found that both molecular and dissociative adsorption can take place with significant charge redistributions. In the present case, we also expect to observe similar adsorption mechanisms for NM and FOX-7 molecules on the Al_2O_3 surface.

As in the case of NM, the first sets of calculations focused on adsorption of the FOX-7 molecule starting from configurations in which the CC bond axis in FOX-7 is initially perpendicular to the surface. Figure 11 presents two such adsorption configurations. Panel a1 of Figure 11 shows an initial configuration of FOX-7 in which the C═C bond of FOX-7 is perpendicular to the surface and one of the O atoms from each nitro group is pointing toward the surface. The O atoms are positioned approximately above one Al atom in the first layer and another Al atom in the second layer of the surface, as indicated by dotted lines in Figure 11, panel a1. Panel b1 of Figure 11 illustrates another initial configuration in which the C═C bond in FOX-7 is oriented at an angle of about 55° from the surface normal and only one nitro group of the molecule points toward the surface, with one of the O atoms positioned above a surface Al atom.

The optimized configurations corresponding to adsorption on the surface starting from the initial structures given in panels a1 and b1 of Figure 11 are shown in panels a2 and b2 and are denoted as FX(**I**) and FX(**II**), respectively. In both instances, adsorption takes place molecularly with formation of new Al−O bonds between one of the O atoms of the nitro group and an Al atom beneath it, with corresponding bond lengths of 1.912−1.920 Å. Internal rotation of the molecules to minimize the repulsive interaction between O atoms of the nitro groups and O atoms of the surface also takes place. The computed adsorption energies for the two configurations are 19.7 and 22.8 kcal/mol, respectively. These values are very close to those obtained for the vertical configurations of nitromethane, NM(**I**), NM(**II**), and NM(**III**), with values in the range 19.1−19.8 kcal/

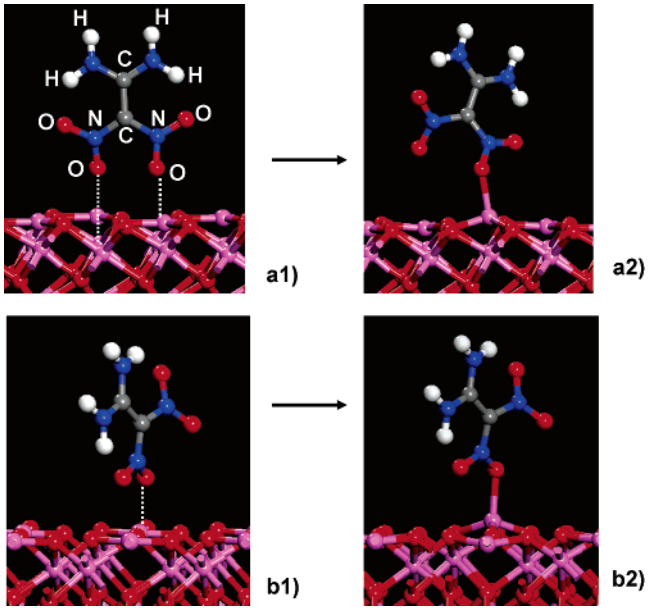

Figure 11. Adsorption configurations FX(**I**) and FX(**II**) of FOX-7 on the $Al_2O_3(0001)$ surface obtained from initial vertical configurations: (a) The C═C bond is perpendicular to the surface, and one of the O atoms from each nitro groups of the molecule are pointing toward the surface. (b) The C═C bond is oriented at about 55° from the surface normal, and only one nitro group of the molecule points toward the surface. The initial configurations are depicted in panels a1 and b1, while the final optimized configurations are presented in panels a2 and b2, respectively.

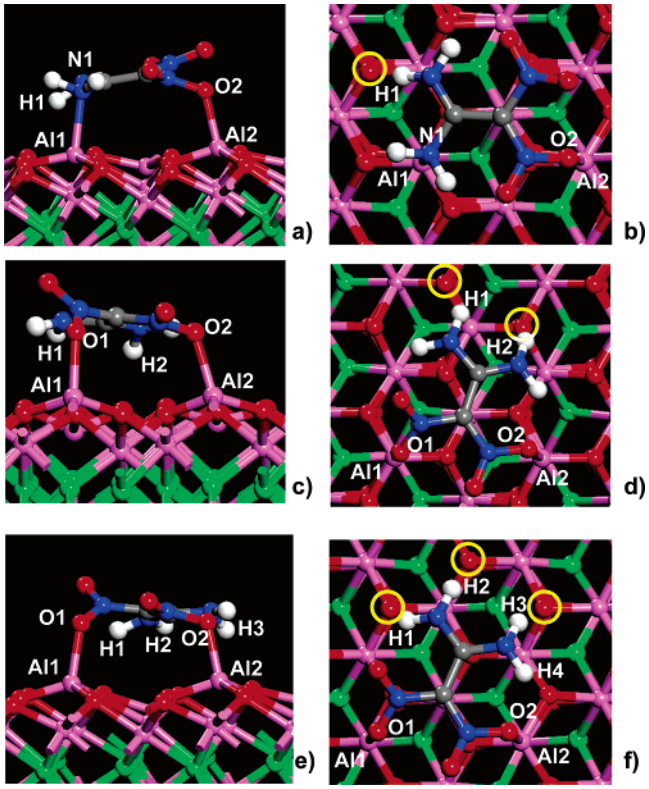

Figure 12. Lateral and top views of the parallel adsorption configurations of the FOX-7 molecule. Panels a, b; c, d; and e, f correspond, respectively, to FX(**III**), FX(**IV**), and FX(**V**) configurations as described in the text.

mol. As a result of adsorption, significant upward dislocation of the Al atoms involved in molecular bonding occurs, with displacements of 0.6 Å for FX(**I**) and 0.63 Å for FX(**II**), respectively.

A second set of configurations in which the FOX-7 molecules are initially oriented parallel to the surfaces also has been investigated. Figure 12 shows three representative parallel adsorption configurations, denoted as FX(**III**), FX(**IV**), and FX(**V**), respectively.

Panels a and b of Figure 12 are lateral and top views of a configuration (FX(**III**)) in which the FOX-7 molecule is adsorbed parallel to the surface such that bonding to surface Al atoms takes place between one of the N atoms of an amine group (denoted as N1) and one of O atoms of a nitro group (denoted as O2). Due to repulsive electrostatic interactions with surface O atoms, the other nitro group is rotated away from the surface toward the vacuum. In this configuration, the N1−Al1 and O2−Al2 bond distances are r(N1−Al1) = 2.10 Å and r(O2−Al2) = 1.945 Å, respectively. In the amine group in which the N atom is bonded to the surface Al atom, there is also an upward pyramidalization of the H atoms. In the other amine group, one H atom (denoted as H1 in Figure 12a) is tilted toward the surface, indicating a hydrogen bond to one of the surface oxygen atoms (indicated with a yellow circle in Figure 12b). The corresponding distance r(H1···O) is 2.131 Å. As a result of the multiple bonds between the FOX-7 molecule and surface, (i.e., the Al−NH_2 and Al−NO_2 bonds as well as the N−H···O−Al hydrogen bond), the adsorption energy is 35.6 kcal/mol, significantly larger than that for the vertical adsorption configuration.

In the FX(**IV**) configuration depicted in panels c and d of Figure 12, the molecular orientation on the surface is such that simultaneous bonding of both nitro groups to the Al surface atoms can take place. One O atom from each nitro group is bonded to an Al surface atom, while the other O atom of each nitro group is rotated away from the surface, due to repulsive electrostatic interactions with the surface O atoms. The corresponding Al−O bond distances are r(Al1−O1) = 1.931 Å and r(Al2−O2) = 1.942 Å. For this configuration, both nitro groups participate in surface bonding, as do both amino groups. Specifically, each amino group has one of its hydrogen atoms involved in hydrogen bonding to the O surface atoms. These O atoms are marked in Figure 12d with yellow circles. The corresponding NH···O hydrogen bonds are 2.49 and 1.857 Å. The total adsorption energy for this configuration is 45.9 kcal/mol.

Finally, panels e and f in Figure 12 show an adsorption configuration in which three of the four H atoms in FOX-7 participate in hydrogen bonds to the surface O-atoms, in addition to formation of an Al−O bond from each of the nitro groups. The hydrogen atoms are denoted as H1, H2, and H3, and the corresponding surface O atoms are identified by yellow circles. The corresponding NH−O bond distances are: r(H1···O) = 2.162 Å, r(H2···O) = 2.317 Å, and r(H3···O) = 2.138 Å, respectively, while the length of the remaining H···O pair is 2.791 Å, larger than the usual range of hydrogen bonds. The Al−O bond lengths are r(Al1−O1) = 1.934 Å and r(Al2−O2) = 1.909 Å, which are similar to the corresponding bond distances in FOX-7(**III**,**IV**). The binding energy of 48.4 kcal/mol is the highest of the five configurations of FOX-7 adsorbed on the $Al_2O_3(0001)$ surface.

The results presented in this section indicate, as in the case of the NM system, the most stable adsorption configurations of the FOX-7 molecule are parallel to the surface. In these cases, multiple bonding can take place. We have identified states in which both nitro and amino groups can be involved in bonding to the surface. The primary bonding takes place through formation of Al−O or Al−N bonds. Additionally, the H atoms

of FOX-7 can form hydrogen bonds to surface O atoms. It should also be noted that FOX-7 also contains intramolecular hydrogen bonds, NH...ON. For example, in the case of the FOX(**V**) structure, the intramolecular hydrogen bond distances have values of 2.341 and 1.896 Å, with O2···H4 corresponding to the shorter bond length (see Figure 12f). Due to the size of the FOX-7 molecule, we have not attempted to determine the activation energies for various bond dissociation channels of this molecule adsorbed on the surface. However, due to the strong interaction with the surface, it is expected that bond dissociation energies will be smaller than those present in the gas phase. This subject will remain open for future study.

IV. Conclusions

The interactions of the NM and FOX-7 molecules with the $Al_2O_3(0001)$ surface have been investigated on the basis of optimizations performed using plane-wave density functional theory calculations with the PW91 exchange-correlation functional.

The first objective of this study was to determine the adsorption mechanisms for these molecular species on the oxide surface. Particularly, our calculations indicate that initial binding takes place through formation of Al−O bonds to the nitro group of NM or one of the nitro groups of FOX-7. The corresponding binding energies for such vertical configurations are similar, with values in the range 19.1−19.8 kcal/mol for NM and 19.7−22.8 kcal/mol for FOX-7. However, for both of these molecular species, the most stable adsorption configurations result when the molecules lay parallel to the surface. For such geometries, the binding energies increase to 26 kcal/mol for NM and 35.6−48.4 for FOX-7. The larger adsorption energies of the FOX-7 molecule are due to the existence of multiple Al−ONO or Al−NH_2 bonds as well as to the formation of one or more NH...O hydrogen bonds with surface oxygen atoms.

The second objective of this work was to identify possible decomposition pathways of NM on the oxide surface and to evaluate the corresponding activation energies. We have determined that, as a result of adsorption on the surface, there are significant variations in the bond dissociation energies of NM relative to the gas phase. Our calculations have indicated that H scission reactions can take place with a small activation energy of about 14 kcal/mol, while in the case of the C−N bond dissociation reaction leading to adsorbed CH_3 and NO_2 fragments, the activation energy is about 38 kcal/mol. Both values are significantly smaller than the corresponding activation energies in the gas phase.

The next objective of this study was to investigate the adsorption properties of various tautomeric forms of NM. In particular, we have analyzed four *aci*-NM tautomers and have determined that, relative to the isolated NM molecule and isolated slab surface, the corresponding adsorption energies are 12.3, 10.5, 19.6, and 13.7 kcal/mol for *aci*-NM(**I**), *aci*-NM(**II**), *aci*-NM(**III**), and *aci*-NM(**IV**), respectively. The minimum energy reaction pathways for H migration from NM(**IV**) with formation of *cis aci*-NM species, or for H migration among different types of *aci*-NM species having *cis* configurations, have also been investigated. We found that the reaction NM(**IV**) → *a*-NM(**III**) has a barrier of about 51 kcal/mol, about 9 kcal/mol smaller than that in the gas phase. In contrast, the H migration reaction *aci*-NM(**III**) → *aci*-NM(**I**) has been found to have an activation energy of about 24.8 kcal/mol, similar to that in the gas phase. However, the reverse reaction *aci*-NM(**I**) → *aci*-NM(**III**) has a smaller activation energy of 17 kcal/mol. The nonequivalent behavior of the two *cis aci*-NM(**I**) and *aci*-NM(**III**) configurations is also reflected by the difference in their binding energies, with the latter energetically preferred by about 8 kcal/mol. Finally, in the case of the *a*-NM(**I**) tautomer, we have also investigated the minimum energy pathway for C−H bond dissociation with subsequent formation of a surface OH group. This process has a barrier slightly larger than that found for direct H-atom elimination from NM, with a value of about 19 kcal/mol. Our calculations also indicate that additional stabilization is provided by the oxide surface for the tautomeric forms *a*-NM(**III**) and *a*-NM(**IV**) in which the OH group is far from the surface. Indeed, the relative energies between the *cis* and *trans a*-NM tautomers and NM decrease by about 5.5 kcal/mol relative to the gas phase when tautomerization takes place on the surface. However, this additional stabilization has not been observed in the case of *a*-NM(**I**) tautomer in which the OH group is close to the surface.

Our final objective was to determine if other nitro-containing molecules such as FOX-7 exhibit adsorption characteristics similar to those of NM. We found, in analogy with the results for NM, a propensity of FOX-7 to adsorb on the surface via formation of Al−O bonds and an energetic preference for formation of parallel, rather than vertical, configurations. However, the parallel conformations of FOX-7 on the aluminum oxide surface also exhibited the ability to form Al−N bonds as well as one or more hydrogen bonds between the amine hydrogen atoms of FOX-7 and surface O atoms.

The validity of the present set of results is restricted to the case of a perfect oxide surface without defective sites. As this is clearly an approximation of the aluminum oxide surface, further investigations to address the influence of the surface defective sites upon the chemisorption and reaction properties of nitro-containing molecules should also be considered in the future.

Acknowledgment. We gratefully acknowledge grants of computer time at the Army Research Laboratory, Aeronautical System Center, the Engineer Research and Development Center, and the Naval Oceanographic Office Major Shared Resource Centers, sponsored by the Department of Defense High Performance Computing Modernization Program. D.L.T. gratefully acknowledges support by the U.S. Army Research Office under grant number DAAD19-01-1-0503.

References and Notes

(1) Sutton, G. P. *Rocket Propulsion Elements*; John Wiley & Sons: New York, 1992.
(2) Politzer, P.; Lane, P.; Grice, M. E. *J. Phys. Chem. A* **2001**, *105*, 7473.
(3) Price, E. W. *Prog. Astronaut. Aeoronaut.* **1984**, *6*, 479.
(4) Kwok, Q. S. M.; Fouchard, R. C.; Turcotte, A. M.; Lightfoot, P. D.; Bowes, R. *Propellants, Explos., Pyrotech.* **2002**, *27*, 229.
(5) Ivanov, G. V.; Tepper, F. In *Challenges in Propellants and Combustion 100 Years After Nobel*; Kuo, K. K., Eds.; Begell House: New York, 1997; p 636.
(6) Yamaguchi, M. *J. Chem. Soc., Faraday Trans.* **1997**, *93*, 3581.
(7) Nesterenko, N.; Lima, E.; Graffin, P.; Charles de Ménorval, L.; Laspéras, M.; Tichit, D.; Fajula, F. *New J. Chem.* **1999**, *23*, 665.
(8) Lima, E.; Charles de Ménorval, L.; Tichit, D.; Laspéras, M.; Graffin, P.; Fajula, F. *J. Phys. Chem. B* **2003**, *107*, 4070.
(9) Allouche, A. *J. Phys. Chem.* **1996**, *100*, 1820
(10) Sorescu, D. C.; Boatz, J. A.; Thompson, D. L. *J. Phys. Chem. B* **2003**, *107*, 8953.
(11) Kresse, G.; Hafner, J. *Phys. Rev.* **1993**, *B48*, 13115.
(12) Kresse, G.; Furthmüller, J. *Comput. Mater. Sci.* **1996**, *6*, 15.
(13) Kresse, G.; Furthmüller, J. *Phys. Rev.* **1996**, *B54*, 11169.
(14) Vanderbilt, D. *Phys. Rev.* **1990**, *B41*, 7892.
(15) Kresse, G.; Hafner, J. *J. Phys.: Condens. Matter* **1994**, *6*, 824.
(16) Perdew, J. P.; Chevary, J. A.; Vosko, S. H.; Jackson, K. A.; Pedersen, M. R.; Singh, D. J.; Frolhais, C. *Phys. Rev.* **1992**, *B46*, 6671.
(17) Monkhorst, H. J.; Pack, J. D. *Phys. Rev.* **1976**, *B13*, 5188.

(18) Kresse, G.; Hafner, J. *Phys. Rev*. **1993**, *B47*, 588.
(19) Jónsson, H.; Mills, G.; Jacobsen, K. W. Nudged elastic band method for finding minimum energy paths of transitions. In C*lassical Quantum Dynamics in Condensed Phase Simulations*; Berne, B. J., Ciccotti, G., Coker, D. F., Eds.; World Scientific: Singapore. 1998; p 385.
(20) Murnaghan, F. D. *Proc. Natl. Acad. Sci. U.S.A.* **1944**, *30*, 2344.
(21) Wyckoff, W. R. G. *Crystal Structures*, 2nd ed.; Interscience: New York, 1964; Vol. 2.
(22) d'Amour, H.; Schiferl, D.; Denner, W.; Schulz, H.; Holzapfel, W. B. *J. Appl Phys.* **1978**, *49*, 4411.
(23) *CRC Handbook of Chemistry and Physics*, 67th ed.; CRC: Boca Raton, FL, 1983.
(24) Manassidis, I.; De Vita, A.; Gillan, M. J. *Surf. Sci. Lett.* **1993**, *285*, L517.
(25) Jarvis, E. A. A.; Carter, E. A. *J. Phys. Chem. B* **2001**, *105*, 4045.
(26) Alavi, S.; Sorescu, D. C.; Thompson, D. L. *J. Phys. Chem. B* **2003**, *107*, 186.
(27) Sorescu, D. C.; Boatz, J. A.; Thompson, D. L. *J. Phys. Chem. A* **2001**, *105*, 5010.
(28) Lammertsma, K.; Prasad, B. V. *J. Am. Chem. Soc*. **1993**, *115*, 2348.
(29) Lammertsma, K.; Prasad, B. V. *J. Am. Chem. Soc.* **1994**, *116*, 642.
(30) Pople, J. A.; Head-Gordon, M.; Fox, D. J.; Raghavachari, K.; Curtiss, L. A. *J. Chem. Phys*. **1989**, *90*, 5622.
(31) Jeffrey, G. A.; Ruble, J. R.; Wingert, L. M.; Yates, J. H.; McMullan, R. K. *J. Am. Chem. Soc*. **1985**, *107*, 6227.
(32) Mulliken, R. S. *J. Chem. Phys*. **1955**, *23*, 1833, 2343.
(33) Delley, B. *J. Chem. Phys*. **1990**, *92*, 508.
(34) Delley, B. *J. Chem. Phys*. **2002**, *113*, 7756.
(35) Perdew, J. P.; Wang, Y. *Phys. Rev.* **1992**, *B45*, 13244.
(36) McKee, M. L. *J. Am. Chem. Soc.* **1986**, *108*, 5784.
(37) Batt, L.; Robinson, G. N. In *The Chemistry of Amino, Nitroso, and Nitro Compounds and their Derivatives*; Patai, S., Ed.; Wiley: New York, 1982.
(38) Latypov, N. V.; Bergman, J.; Langlet, A.; Wellmar, U.; Bemm, U. *Tetrahedron* **1998**, *54*, 11525.